Geometry of polygonal hydraulic jumps and the role of hysteresis

Taylor E. Nichols ⬡ and Joshua B. Bostwick ⬡ [*]

Department of Mechanical Engineering, Clemson University, Clemson, South Carolina 29631, USA

An impinging liquid jet impacts a target plate, forming a hydraulic jump that can exhibit a steady polygonal geometry under a range of conditions. Experiments are conducted to determine the effect of weir geometry and flow history on mode selection and the geometry of these polygonal jumps. Modal transitions occur at different flow rates in upscale and downscale flow sweeps, leading to hysteresis and the coexistence of multiple modes at a given flow rate, illustrating the importance of flow history. The characteristic ratio A/PH or normalized jump geometry, where A is the upstream area of the jump, P is the perimeter, and H is the downstream height, is unaffected by the flow history or experimental protocol but has a slight dependence on the weir height h_w and weir radius r_w provided the ratio of the weir radius to nozzle radius r_n is large, $r_w/r_n \geqslant 28$. The collapse of the geometry suggests surface tension plays a critical role in the formation of polygonal jumps. All of our data, approximately 1800 observations, collapse upon plotting the scaled perimeter P/H with the downstream Weber number We, and we show the critical wavelength is approximately constant λ/H for any given experiment, suggesting the mode selection mechanism is related to Plateau-Rayleigh breakup.

I. INTRODUCTION

Circular hydraulic jumps are formed when a liquid jet impacts a horizontal plate, which creates a radial flow that abruptly changes height at a critical radius. Predictions for that critical radius were given by Rayleigh [1] for an inviscid fluid, which was improved by Watson [2] to account for liquid viscosity and the plate boundary layer, which agreed with experimental observations to a varying extent [3–9]. Bush and Aristoff [10] extended Watson's theory to account for small surface tension effects near the jump circumference and demonstrated the jump radius can be increased through the use of surfactant to lower the surface tension. However, it was not until Bhagat *et al.* [11] showed surface tension and viscous forces balance the momentum at the jump (independent of gravitational effects) that the critical radius for circular jumps was well understood. In contrast, the stability of circular hydraulic jumps is not as well understood. Ellegaard *et al.* [12,13] showed in a beautiful experiment that the steady circular hydraulic jump can lose stability and form striking polygonal shapes under a particularly small range of experimental conditions, highlighting the sensitive dependence between fluid inertia, viscosity, and surface tension effects. In this paper, we perform a careful experimental study of polygonal hydraulic jumps and are interested in documenting the role of flow history (experimental protocol) and weir geometry on mode selection and the resulting polygonal jump geometry.

Observations of asymmetric instabilities in circular jumps were documented [7,14] prior to the discovery of steady polygonal jumps by Ellegaard *et al.* [12,13], and since then, there have been numerous discoveries of complex geometric structures in circular hydraulic jumps, which

---

[*]jbostwi@clemson.edu; https://cecas.clemson.edu/~jbostwi/

include the hydraulic bump [15], the clover regime [16], and steady rotating polygonal jumps [17]. Steady polygonal jumps have also been observed on microdecorated surfaces [18], micropatterned surfaces [19], and rotating surfaces [20]. The transition from symmetric to asymmetric structures is typically preceded by a roller vortex downstream of the jump [21–24], and Labousse and Bush [25] theoretically investigated the role of this toroidal vortex in the formation of polygonal jumps, the hydraulic bump, and the Leidenfrost torus [26]. More generally, it is believed that mode number selection in polygonal hydraulic jumps is related to Plateau-Rayleigh breakup, a capillary phenomenon, and this was demonstrated in experiments by Bush *et al.* [16] where a polygonal jump is destroyed by introducing surfactant into the system which sufficiently lowers the surface tension of the liquid. Models have been put forth to predict the transition from circular to polygonal jump geometry, which include the phenomenological model by Martens *et al.* [27] and the inertial lubrication models of Rojas *et al.* [28], Rojas and Tirapegui [29].

The difficulty in relating the geometry of polygonal jumps to Plateau-Rayleigh breakup of a cylinder is the secondary curvature inherent in the toroidal geometry of the jump. This dependence on the secondary curvature is seen in experiments on liquid toroids in Newtonian fluids [30], polymers [31], and yield stress materials [32] and also appears explicitly in theoretical models of capillary breakup of toroids [33,34]. Polygonal instabilities on toroidal surfaces have also been observed in the Leidenfrost state [26,35]. In classical Plateau-Rayleigh breakup of a liquid cylinder, instability is driven by geometry as the cylinder breaks up into spherical drops to minimize surface area. Our experimental data collapses when plotting the jump perimeter scaled by the downstream jump height against the downstream Weber number, also showing the importance of geometry in the formation of polygonal jumps.

Lastly, polygonal hydraulic jumps are interesting from a pedagogy perspective as they illustrate the concept of hydrodynamic instability, i.e., competition between forces, in a table-top experiment that can be used in classroom demonstrations. As stated earlier, the phenomenon occurs over a small range of parameters, and it is important to achieve precise experimental conditions to observe polygonal jumps. We aim to provide these details in our description of the experimental setup for ease of reproducibility by the community. For example, we observed that a pulseless flow is required to achieve steady jumps and that small irregularities in weir height around the perimeter resulted in asymmetric shapes, to name a few details. Furthermore, we document two experimental protocols, (i) natural state and (ii) upscale-downscale, and show how they yield different results for all other experimental conditions fixed. Weir geometry is also important to the extent that it affects the downstream jump height, and we show this using weirs with circular and square geometry.

We begin this paper by describing in detail the experimental protocol to create polygonal hydraulic jumps and the image processing and measurement techniques required to accurately describe the jump geometry. Two flow protocols, (i) natural state and (ii) upscale-downscale, are contrasted for a fixed set of experimental parameters, and we show the existence of hysteresis for a given mode number N in the upscale-downscale case. Even though mode selection is affected by the protocol, the jump geometry as defined by the characteristic ratio A/PH is not, and we show how that ratio depends upon the weir height h_w and weir geometry through the radius r_w for circular weirs and the edge length L_w for square weirs. We show the scaled jump perimeter P/H scales with the downstream Weber number We and collapses all of our geometric data onto a master curve. We use this collapse of the data to show the scaled wavelength $\lambda/H \approx 3$, concluding that the mode selection mechanism is related to Plateau-Rayleigh breakup. Lastly some concluding remarks are offered.

II. EXPERIMENT

Hydraulic jumps are created by the experimental apparatus shown in Fig. 1(a). Fluid flows through a nozzle of radius a with flow rate Q at a height h_N above a glass plate with prescribed geometry, either circular with radius r_w or square with edge length L_w. After the fluid impacts the plate it flows radially outward over a weir of h_w and into the recirculation catch tank, which allows
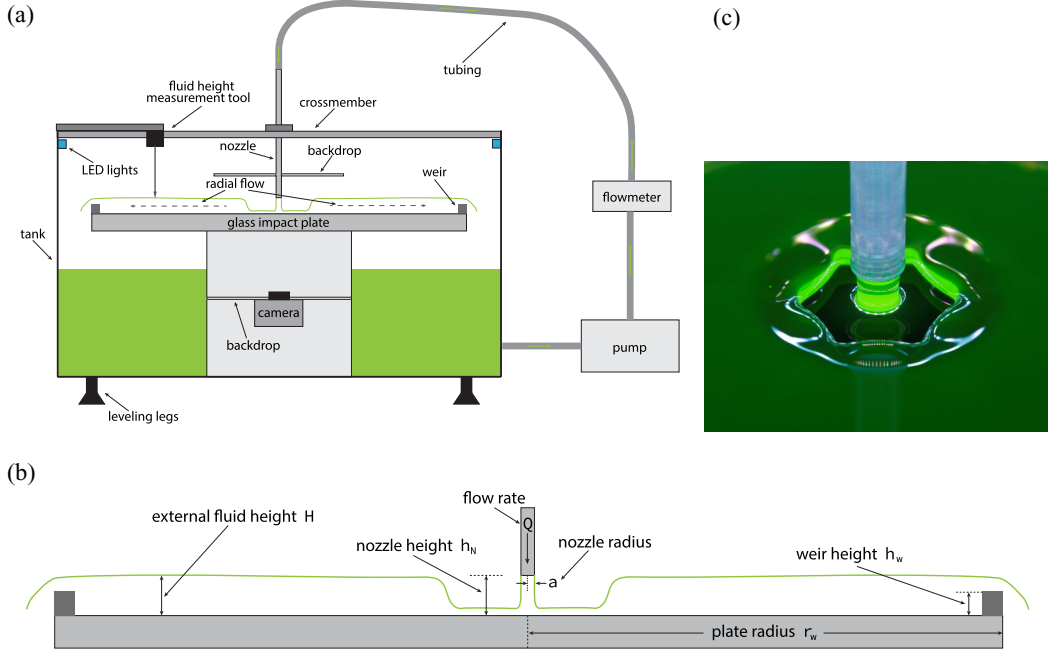
FIG. 1. Experiment: (a) schematic diagram, (b) close-up view of the hydraulic jump, and (c) typical polygonal hydraulic jump.

it to flow in a closed loop. Note that to create the "free-fall effect" the weir is placed at the outer edge of the plate. A hydraulic jump forms in the fluid upstream of the weir, as shown in Fig. 1(b). For a certain set of experimental parameters, asymmetric polygonal hydraulic jumps are formed [see Fig. 1(c)]. These steady structures are extremely delicate and require precise control of the experimental conditions to observe.

Commercial antifreeze (ethylene glycol) was used as the working liquid. The density $\rho = 1.12 \text{ g/cm}^3$ was measured using an Anton-Paar DMA 35 density meter, viscosity $\nu = 13.7-16.4 \text{ mm}^2/\text{s}$ was measured with an Anton Paar MCR-302 rheometer, and surface tension $\sigma = 44 \text{ mN/m}$ was measured using a CSC tensiometer. A centrifugal pump (Iwaki MD-30RT-115NL) circulates the fluid at a flow rate in the range $Q = 30-110 \text{ mL/s}$ and was chosen to create pulseless flow, which is critical in creating the polygonal structures. A Variac (or autotransformer) delivers a variable output voltage to the pump, which changes the impeller speed, thereby allowing for fine flow rate adjustment in increments of $\approx 1 \text{ mL/s}$. The flow rate was measured using a flow meter consisting of a calibrated Digiten FL-408 paddle sensor with a maximum error of 1 mL/s. The plate was measured horizontal, and the nozzle was measured vertical to within $0.01°$ using a DXL360S dual + axis digital protractor, such that the jet impact was normal to the plate. The nozzle had sufficient length that the flow was fully developed and laminar. We have experimented with tapered nozzles, consistent with previous work [16,36–38], but found no noticeable differences between nozzles with and without a taper. The nozzle radius $a = 0.46 \text{ cm}$ and nozzle height $h_N = 1.0 \text{ cm}$ were kept fixed throughout our experiments. Scaling lengths with a gives a Bond number Bo $\equiv \rho g a^2/\sigma = 5.28$ and jet Reynolds number Re $\equiv Q/\nu a = 450-1350$ in our experiments. Note that since we use a single fluid in our experiments, we report our results in terms of flow rate Q instead of Re.

Glass target plates were used because of their uniform thickness, smooth surface, and transparency. Weirs were affixed to the outer edge of plates with (i) circular geometry of radius $r_w = 7.6, 12.7, 15.2, 17.8 \text{ cm}$ and (ii) square geometry of edge length $L_w = 22 \text{ cm}$. Each weir geometry
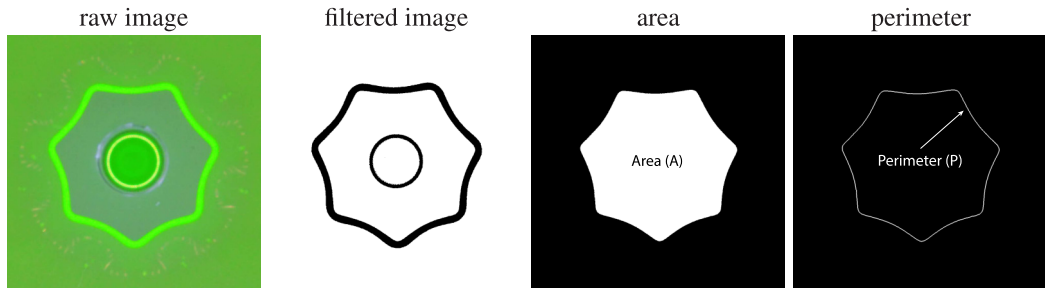
FIG. 2. Image processing routine takes a raw image and filters it, from which the area A and perimeter P can be extracted.

was precision three-dimensionally printed in four separate heights, $h_w = 2.67, 2.84, 3.17, 3.4$ mm (three for the square weirs, 2.84, 3.17, 3.4 mm), and fine-grit sand paper was used to ensure the weir height was uniform along the perimeter. To measure the downstream fluid height H, we utilize a method by Ellegaard *et al.* [39], Rao and Arakeri [40] which consists of vertically translating a current-conducting rod using a stepper motor into the fluid, at which point an electrical signal is recognized. We measure the fluid height 3 cm inside the weir for consistency. The range of heights we report is $H = 5.50$–6.52 mm.

The geometry of the polygonal hydraulic jump is imaged from beneath the glass plate and results in the typical image shown in Fig. 2. Light-emitting diode (LED) lighting is used to accentuate the boundary of the jump. The jump geometry is characterized by the external height H, previously discussed, and the area A and perimeter P of the planar shape. We summarize the image processing technique to compute A and P. A raw image is taken from beneath the target plate, centered, and the resulting image is filtered into a black-and-white image (filtered image). The inner portion of the filtered image is isolated, and the white pixels are counted to extract the area of the structure. Edge detection is used to determine the perimeter. The calculated values of A and P are found using a calibration based on known geometries beforehand. To summarize, a polygonal hydraulic jump is characterized by the mode number N, downstream height H, area A, and perimeter P.

Two distinct experimental protocols are used, (i) upscale-downscale and (ii) the natural state, which highlights the role of hysteresis and flow history in the formation of polygonal hydraulic jumps. The goal of the upscale-downscale protocol is to determine the range of flow rates for which a given mode number N is possible. The upscale portion of the protocol begins by slowly increasing the flow rate until a steady jump appears. This is typically the $N = 3$ shape. The flow rate is then increased in small increments, ≈ 1 mL/s, and data is collected at each step, but the jump is not interfered with. We continue to increase the flow rate until the jump becomes unsteady, which typically occurs for the $N = 10$ mode. The downscale portion of the protocol begins at the highest flow rate that achieves a steady jump, and the flow is decreased in small increments until the jump collapses into the fluid jet. The range in flow rate for which a given mode N exists will be referred to as the hysteresis ΔQ. The natural-state protocol differs in that at a given flow rate the jump is destroyed by a glass probe and allowed to relax into its preferred geometry. Here it is important to use small increments, as the transition from $N \rightarrow N + 1$ does not always happen suddenly and under certain conditions multiple shapes N exist for a given flow rate.

III. RESULTS

We report experimental observations of polygonal hydraulic jumps and highlight the role of (i) weir geometry h_w, r_w and (ii) the experimental protocol on the jump geometry (N, H, A, P). We begin by contrasting mode number selection in the two experimental protocols and characterize the hysteresis as it depends upon the weir height. The normalized jump geometry A/PH is shown to be
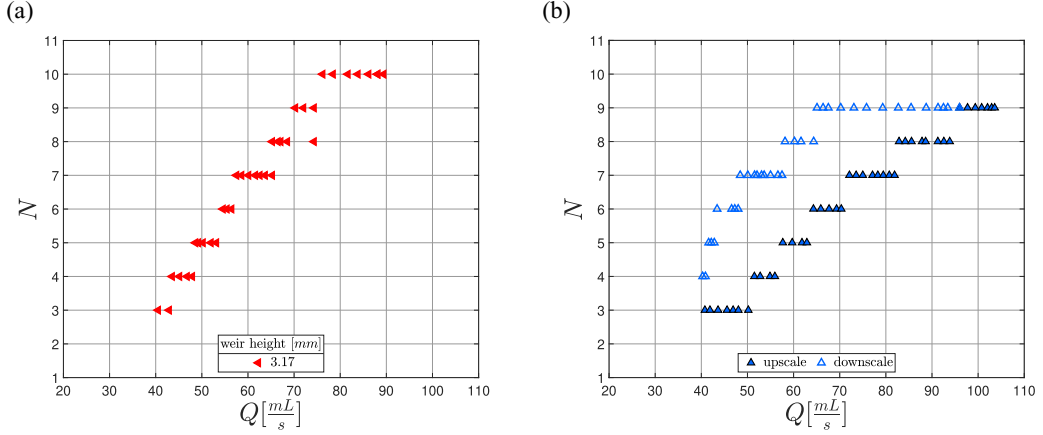
(a)

(b)

FIG. 3. Mode number N against flow rate Q contrasting the (a) natural state and (b) upscale-downscale protocols for a weir with $h_w = 3.17$ mm and $r_w = 17.8$ cm.

unaffected by the particular protocol but does depend upon the weir geometry, and we characterize this dependence. All of our data, approximately 1800 observations of polygonal jumps, collapse with the downstream Weber number using H as the characteristic length scale. Lastly, we show the scaled wavelength approaches a constant value, leading us to believe the mode selection mechanism is related to the Plateau-Rayleigh instability.

A. Experimental protocol

Figure 3 contrasts the natural state and upscale-downscale protocols by plotting the mode number N against flow rate Q for the same weir. In both cases, the mode number N increases with the flow rate Q, and for the natural-state protocol that trend appears to be linear [see Fig. 3(a)]. Interestingly, for higher mode numbers, multiple shapes are observed for a given flow rate in the natural-state protocol. For example, Fig. 3(a) shows that for $Q \approx 62$ mL/s, it is possible to observe $N = 7, 8, 9$ modes. That is, mode selection is not unique, despite the fact that the natural-state protocol requires the destruction of the prior shape before the relaxation of the jump into the lowest-energy state. We assume these regions correspond to the boundary of the domain of attraction between two or more modes. Lastly, we note that jump asymmetry was not common in the natural-state experiments but did occur more frequently in these overlap regions.

In the upscale-downscale protocol, modal transitions occur when $N \to N + 1$ during the upscale sweep and $N \to N - 1$ during the downscale sweep, as shown in Fig. 3(b). For a given mode N, the upscale and downscale transitions occur at different flow rates, and this difference increases with mode number. This difference illustrates hysteresis ΔQ, which we define as the difference between the maximum flow rate during the upscale sweep and the minimum flow rate during the downscale sweep for a given mode number. At a given flow rate Q more than one mode can exist, and for $58 < Q < 70$ mL/s there are four potential modes. Figure 4 shows the mode shapes at the transitions in the upscale and downscale sweeps. Here we note that for each polygonal shape there is a ring vortex ("roller") downstream of the jump that is best seen in the entrained bubbles adjacent to the polygon sides in the upscale sweep of Fig. 4, consistent with prior experimental observations [21–25]. Within the vortex, there is a slow azimuthal flow towards the corners where a strong jet expels the liquid downstream that can easily be seen by adding dye to the fluid directly downstream of the jump [27]. In the upscale sweep, the area A and perimeter P of the shape will increase, and the mode will transition from $N \to N + 1$. Typically, we observe that one or more sides of the polygon become either asymmetric or convex before transition. During the downscale sweep, the sides are
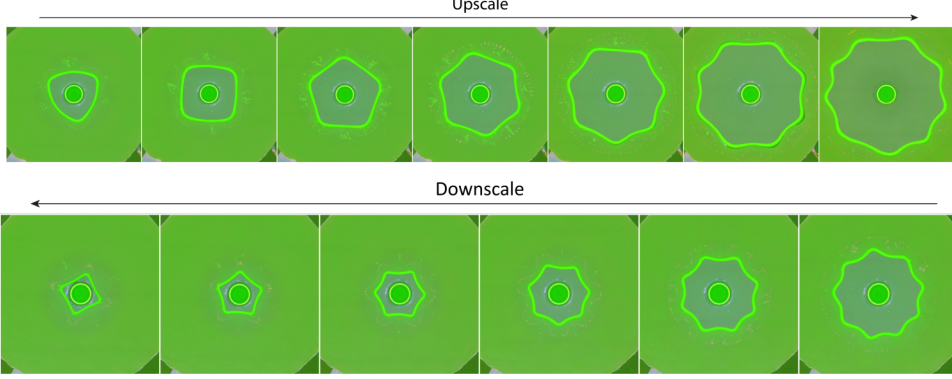
FIG. 4. Mode shapes at the transition for the upscale-downscale experiment, shown in Fig. 3(b), for a weir with $h_w = 3.17$ mm and $r_w = 17.78$ cm.

typically concave, and the shape decreases in size until one of the corners becomes small enough that the rotating vortices there interact with one another, leading to a collapse of the corner and therefore $N \to N - 1$.

Figure 5 plots the mode number N against the hysteresis ΔQ, as it depends upon the weir height h_w. The trend is similar for low mode numbers, $N = 3$–6, but starts to deviate for $N \geqslant 7$, with the taller weirs which we attribute to the larger flow rate (equivalently, inertia) required to create such shapes.

B. Geometry of the jump

For each data point the flow rate Q, mode number N, area A, perimeter P, and external height H are determined. This information allows us to completely characterize the geometry of the polygonal hydraulic jump. As we have shown, the experimental protocol is important in mode
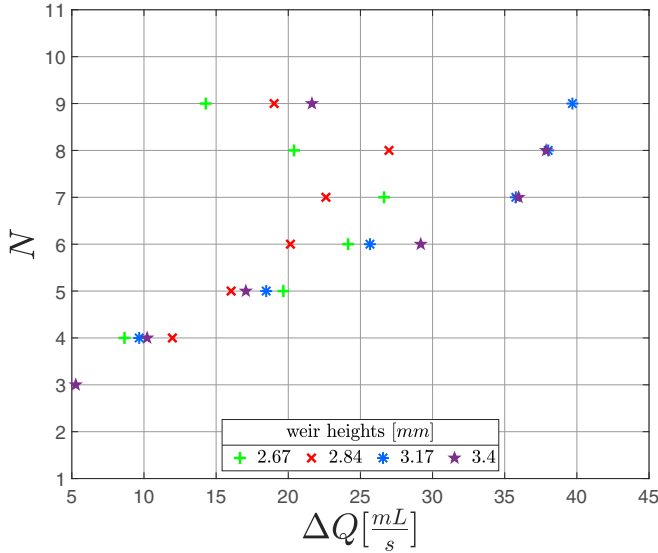

FIG. 5. Mode number N against hysteresis ΔQ as it depends upon weir height h_w for fixed $r_w = 17.8$ cm in the upscale-downscale experiment.
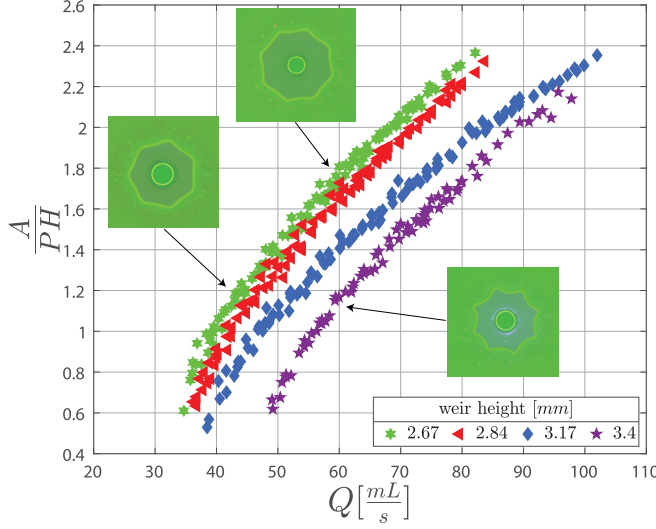
FIG. 6. Characteristic ratio A/PH against flow rate Q as it depends upon weir height h_w for the $r_w = 17.78$ cm plate for the natural state and upscale-downscale data. Inset images for $Q = 60$ mL/s show the difference in the $N = 8$ mode between $h_w = 2.67$ mm and $h_w = 3.4$ mm.

number selection, and we investigate if the jump geometry is similarly affected. To do so, we introduce the characteristic ratio A/PH, or scaled area, which is the ratio of the projected area of the upstream region of the jump A to the surface area of the transition region of the jump PH, where the curvature is the highest. Figure 6 plots the characteristic ratio A/PH against flow rate Q for both natural-state and upscale-downscale data. Interestingly, for a fixed weir height h_w all the data collapse to a single curve, indicating the geometric number A/PH is independent of shape for given flow conditions. For increasing weir height h_w, the curve is shifted to the right, indicative of the larger flow rate required to make a shape with similar geometry. This also tends to correspond to a change in mode number; for example, for $A/PH = 1.2$ the mode number increases, and the shape becomes more concave. The contrast between shapes for a fixed flow rate $Q = 60$ mL/s is similarly striking, showing that for higher h_w the sides become more concave but the mode number is constant.

C. Weir geometry

In previous experimental studies, it has not been clear whether the weir geometry outside of the weir height h_w affected modal behavior. To investigate this we experimented with circular weirs of varying radius $r_w = 7.2$–17.2 cm and a square weir with edge length $L_w = 22$ cm. In all cases, the weir was affixed to the outer edge of the plate to create the free-fall effect. Figure 7(a) plots the mode number N against flow rate Q for a fixed weir height $h_w = 2.84$ mm and varying weir geometry in the natural-state experiments, showing the data for the circular weirs generally overlap one another, whereas the data for the square weir differ from the circular weirs. This indicates there is some effect, albeit small, of weir geometry on mode selection in the natural-state protocol. This is most likely related to the breaking of the circular symmetry of the flow over the weir, which would be akin to angular modulations of the weir height. Figure 7(b) plots the characteristic ratio A/PH against flow rate Q, showing a collapse of the same data for all weir geometries.

Weir geometry becomes important when the jump radius becomes comparable to the weir radius. Figure 8 plots the mode number N against flow rate Q in an upscale-downscale experiment, comparing our largest radius weir ($r_w = 17.8$ cm) to our smallest radius weir ($r_w = 7.62$ cm),
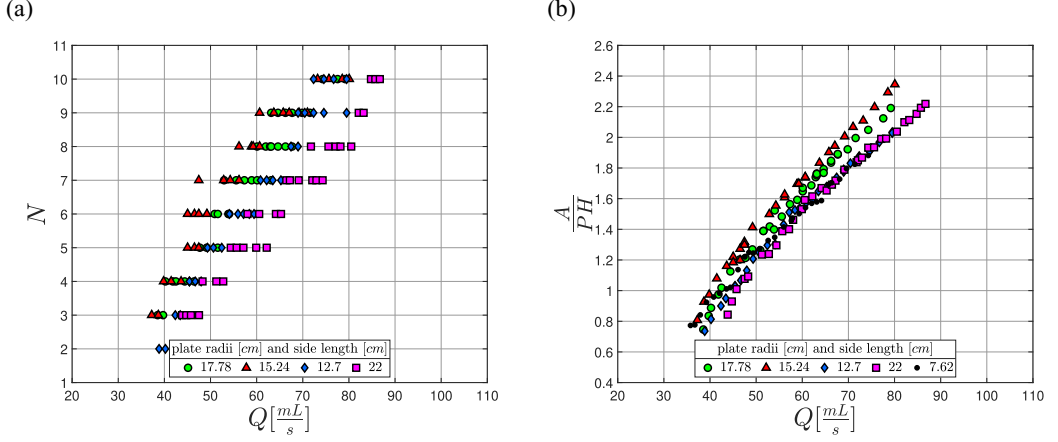
(a)

(b)

FIG. 7. Weir geometry: (a) mode number N and (b) characteristic ratio A/PH against flow rate Q for $h_w = 2.84$ mm, as it depends upon the weir geometry, during the natural-state experiment. Weirs are either circular with a prescribed radius r_w or square with a prescribed edge length.

which is comparable in size to a typical jump. It is interesting to note that the downscale sweep is relatively unaffected by the weir radius, but the upscale sweep shows a dramatic difference with the smaller-radius weir, exhibiting modal transitions at much smaller flow rate than the larger weir radius. This difference suggests weir radius plays a role when the scale of the jump is comparable in magnitude to the scale of the weir. We observed that for a ratio of weir to nozzle radius $r_w/r_N \geqslant 28$ the results are indistinguishable, but there are notable differences when $r_w/r_N = 16.5$.

As discussed previously, the characteristic ratio A/PH is independent of mode number, weir geometry, and the experimental protocol but does depend upon weir height h_w. This suggests the downstream fluid height is the relevant length scale, and we introduce the downstream Weber
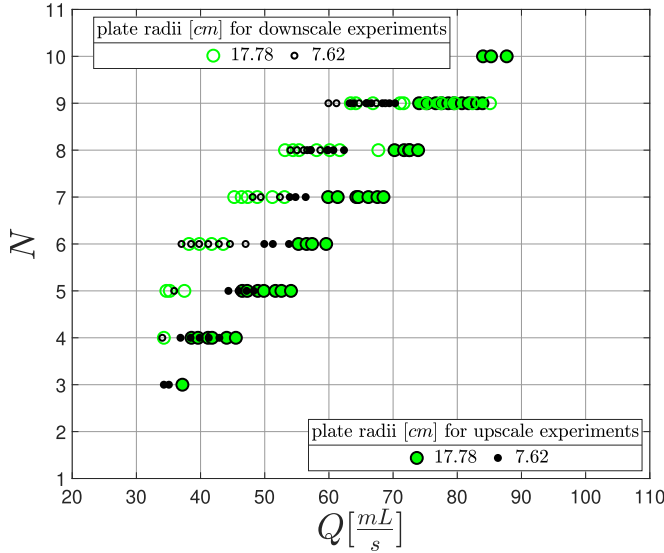

FIG. 8. Mode number N against flow rate Q in the upscale-downscale experiment with $h_w = 2.84$ mm contrasting the largest ($r_w = 17.8$ cm) and smallest ($r_w = 7.6$ cm) radius weir.
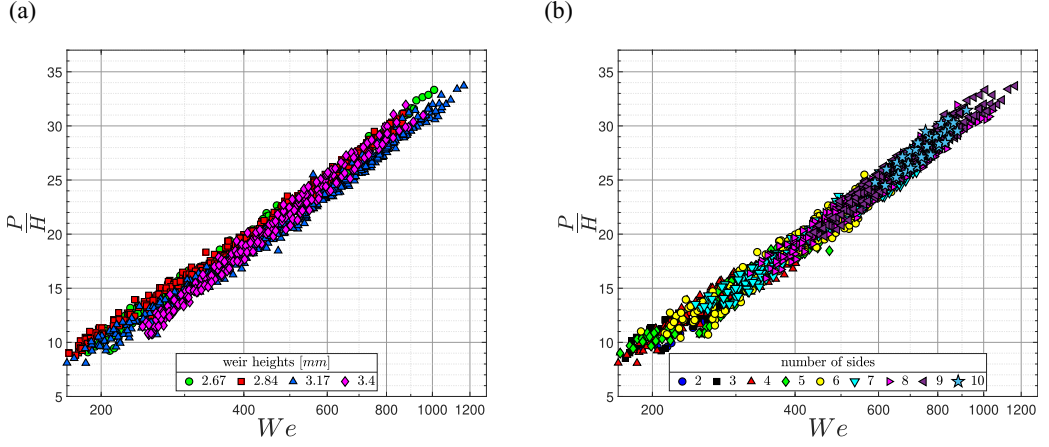
(a)

(b)

FIG. 9. Scaled perimeter P/H against the downstream Weber number We for all data as it depends upon (a) weir height h_w and (b) mode number N.

number We $\equiv \rho Q^2/\gamma H^3$. Figure 9 plots the scaled perimeter P/H against We for all of the data, approximately 1800 experiments, and shows a nice collapse. In general, higher mode numbers N are associated with larger Weber numbers We, but there is a finite range where those modes can be observed, which is related to the hysteresis seen in the upscale-downscale experiments [see Fig. 9(b)].

D. Critical wavelength

The collapse of our data for the jump geometry with Weber number We suggests that mode number selection is determined by the competition between fluid inertia and surface tension forces. A similar competition is seen in Plateau-Rayleigh breakup of a liquid jet, and we investigate whether a similar mechanism is responsible for polygonal hydraulic jumps. The difference is that our polygonal jump exhibits a weak secondary curvature of the toroidal geometry. We define the wavelength as $\lambda \equiv P/N$ and plot the scaled wavelength λ/H against mode number N in Fig. 10 for
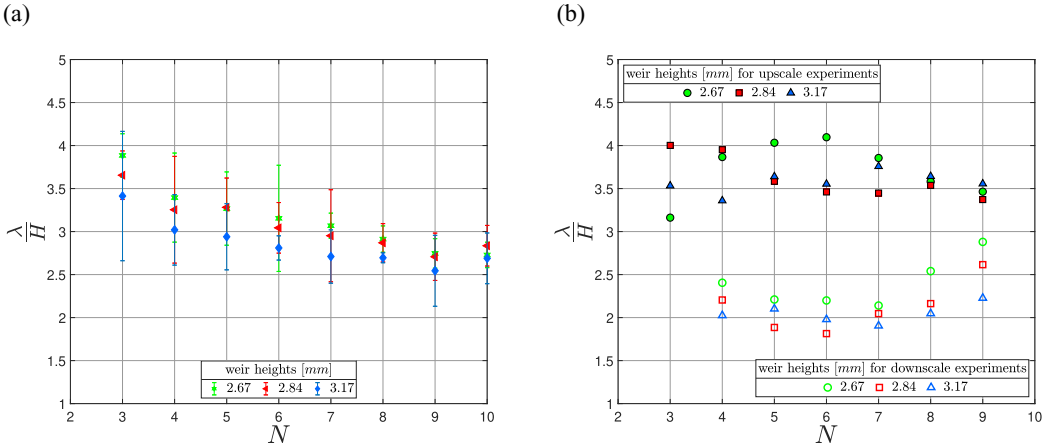
(a)

(b)

FIG. 10. Scaled wavelength λ/H against mode number N for the (a) natural state and (b) upscale-downscale experiments with $r_w = 17.8$ cm, depending upon weir height h_w.

the natural-state and upscale-downscale experiments, as it depends upon the weir height. Our data show the weir height does not affect the critical wavelength. The difference in critical wavelength during the upscale and downscale sweeps is presumably related to hysteresis [see Fig. 10(b)]. For the natural-state experiments, the scaled wavelength $\lambda/H \approx 3$ is approximately constant, consistent with the Plateau-Rayleigh instability mechanism where the critical scaled wavelength is constant and depends upon the radius of the liquid cylinder, which would correlate to the downstream height H in our toroidal geometry. The small deviation of λ/H with mode number N suggests a weak dependence upon another parameter, which might include the secondary curvature of the toroidal shape, which becomes more important for smaller mode numbers. This dependence has been observed in the breakup of liquid toroids [30].

IV. CONCLUDING REMARKS

An experimental study of polygonal hydraulic jumps was performed, resulting in the observation of approximately 1800 steady-state polygonal structures. Our focus was on the role of experimental protocol and weir geometry in the formation of polygonal jumps. For each observation, we quantified the mode number N, perimeter P, area A, and downstream fluid height H of the jump, as it depended upon the weir geometry through the height h_w and radius r_w. Two protocols were defined, (i) the natural state and (ii) upscale-downscale, to observe the transition between modal behaviors. For the upscale-downscale experiments, we observed hysteresis ΔQ in mode number selection and multiple modes existing at the same flow rate. Surprisingly, we found the jump geometry, as defined by the characteristic ratio A/PH, is unaffected by the experimental protocol and weir geometry, provided the ratio of weir to nozzle radius $r_w/r_N \geqslant 28$, but has a weak dependence upon the weir height h_w. All of our data collapse against the downstream Weber number We, suggesting the downstream height is the relevant length scale.

Scaling the wavelength with downstream height shows a collapse to an approximately constant value $\lambda/H \approx 3$, suggesting the modal selection mechanism is related to the Plateau-Rayleigh instability of a liquid column, which exhibits a constant scaled wavelength, irrespective of mode. This conclusion was previously reported, and our results further support the perspective that surface tension is important in the formation of polygonal hydraulic jumps [16,41]. Our scaled wavelength differs slightly from the Plateau-Rayleigh prediction of $\lambda/H = 4.5$, and we attribute this difference to a number of factors that influence this constant, such as the introduction of a secondary curvature in the toroidal geometry compared to the cylinder and the role of viscosity in defining the critical wavelength. This shift in critical wavelength is also seen in Plateau-Rayleigh breakup of liquid rivulets [42] and liquid toroids [33]. As mentioned by Pairam and Fernández-Nieves [30] for a toroidal donut, the major and minor radii evolve from an initial shape by expanding or contracting until a critical value is reached, upon which the donut pinches off in the critical wavelength. Note that the hydraulic jump geometry is unable to spontaneously expand or contract to adopt a preferred geometry, and perhaps for this reason there is a range of preferred λ/H that we see in experiment. This is best seen in the upscale-downscale experiments, which exhibit different critical wavelengths for the maximum and minimum modes [see Fig. 10(b)]. Even so, there is a mild collapse of the data for these states, indicating that polygonal hydraulic jumps are a geometric phenomenon governed by a complex balance between surface tension, viscosity, and fluid inertia.

ACKNOWLEDGMENTS

---

[1] L. Rayleigh, On the theory of long waves and bores, Proc. R. Soc. London, Ser. A **90**, 324 (1914).

[2] E. J. Watson, The radial spread of a liquid jet over a horizontal plane, J. Fluid Mech. **20**, 481 (1964).

[3] R. G. Olsson and E. T. Turkdogan, Radial spread of a liquid stream on a horizontal plate, Nature (London) **211**, 813 (1966).

[4] S. Ishigai, S. Nakanishi, M. Mizuno, and T. Imamura, Heat transfer of the impinging round water jet in the interference zone of film flow along the wall, Bull. JSME **20**, 85 (1977).

[5] V. E. Nakoryakov, B. G. Pokusaev, and E. N. Troyan, Impingement of an axisymmetric liquid jet on a barrier, Int. J. Heat Mass Transfer **21**, 1175 (1978).

[6] M. Bouhadef, Étalement en couche mince d'un jet liquide cylindrique vertical sur un plan horizontal, Z. Angew. Math. Phys. **29**, 157 (1978).

[7] A. D. D. Craik, R. C. Latham, M. J. Fawkes, and P. W. F. Gribbon, The circular hydraulic jump, J. Fluid Mech. **112**, 347 (1981).

[8] M. Errico, A study of the interaction of liquid jets with solid surfaces, Ph.D. thesis, University of California, San Diego, 1986.

[9] V. K. Vasista, Experimental study of the hydrodynamics of an impinging liquid jet, Ph.D. thesis, Massachusetts Institute of Technology, 1989.

[10] J. W. M. Bush and J. M. Aristoff, The influence of surface tension on the circular hydraulic jump, J. Fluid Mech. **489**, 229 (2003).

[11] R. K. Bhagat, N. K. Jha, P. F. Linden, and D. I. Wilson, On the origin of the circular hydraulic jump in a thin liquid film, J. Fluid Mech. **851**, R5 (2018).

[12] C. Ellegaard, A. E. Hansen, A. Haaning, K. Hansen, A. Marcussen, T. Bohr, J. L. Hansen, and S. Watanabe, Creating corners in kitchen sinks, Nature (London) **392**, 767 (1998).

[13] C. Ellegaard, A. E. Hansen, A. Haaning, K. Hansen, A. Marcussen, T. Bohr, J. L. Hansen, and S. Watanabe, Cover illustration: Polygonal hydraulic jumps, Nonlinearity **12**, 1 (1999).

[14] X. Liu and J. H. Lienhard, The hydraulic jump in circular jet impingement and in other thin liquid films, Exp. Fluids **15**, 108 (1993).

[15] M. Labousse and J. W. M. Bush, The hydraulic bump: The surface signature of a plunging jet, Phys. Fluids **25**, 094104 (2013).

[16] J. W.M. Bush, J. M. Aristoff, and A. E. Hosoi, An experimental investigation of the stability of the circular hydraulic jump, J. Fluid Mech. **558**, 33 (2006).

[17] A. R. Teymourtash, M. Khavari, and M. Passandideh Fard, Experimental and numerical investigation of circular hydraulic jump, in ISME2010 (unpublished).

[18] E. Dressaire, L. Courbin, Jérome Crest, and Howard A. Stone, Thin-Film Fluid Flows over Microdecorated Surfaces: Observation of Polygonal Hydraulic Jumps, Phys. Rev. Lett. **102**, 194503 (2009).

[19] M. Johnson, D. Maynes, and J. Crockett, Experimental characterization of hydraulic jump caused by jet impingement on micro-patterned surfaces exhibiting ribs and cavities, Exp. Thermal Fluid Sci. **58**, 216 (2014).

[20] T. R. N. Jansson, M. P. Haspang, K. H. Jensen, P. Hersen, and T. Bohr, Polygons on a Rotating Fluid Surface, Phys. Rev. Lett. **96**, 174502 (2006).

[21] T. Bohr, C. Ellegaard, A. E. Hansen, and A. Haaning, Hydraulic jumps, flow separation and wave breaking: An experimental study, Phys. B (Amsterdam, Neth.) **228**, 1 (1996).

[22] T. Bohr, V. Putkaradze, and S. Watanabe, Averaging Theory for the Structure of Hydraulic Jumps and Separation in Laminar Free-Surface Flows, Phys. Rev. Lett. **79**, 1038 (1997).

[23] S. Watanabe, V. Putkaradze, and T. Bohr, Integral methods for shallow free-surface flows with separation, J. Fluid Mech. **480**, 233 (2003).

[24] A. Andersen, T. Bohr, and T. Schnipper, Separation vortices and pattern formation, Theor. Comput. Fluid Dyn. **24**, 329 (2010).

[25] M. Labousse and J. W. M. Bush, Polygonal instabilities on interfacial vorticities, Eur. Phys. J. E **38**, 113 (2015).

[26] S. Perrard, Y. Couder, E. Fort, and L. Limat, Leidenfrost levitated liquid tori, Europhys. Lett. **100**, 54006 (2012).

[27] E. A. Martens, S. Watanabe, and T. Bohr, Model for polygonal hydraulic jumps, Phys. Rev. E **85**, 036316 (2012).

[28] N. Rojas, M. Argentina, and E. Tirapegui, A progressive correction to the circular hydraulic jump scaling, Phys. Fluids **25**, 042105 (2013).

[29] N. Rojas and E. Tirapegui, Harmonic solutions for polygonal hydraulic jumps in thin fluid films, J. Fluid Mech. **780**, 99 (2015).

[30] E. Pairam and A. Fernández-Nieves, Generation and Stability of Toroidal Droplets in a Viscous Liquid, Phys. Rev. Lett. **102**, 234501 (2009).

[31] J. D McGraw, J. Li, D. L. Tran, A.-C. Shi, and K. Dalnoki-Veress, Plateau-Rayleigh instability in a torus: Formation and breakup of a polymer ring, Soft Matter **6**, 1258 (2010).

[32] E. Pairam, H. Le, and A. Fernández-Nieves, Stability of toroidal droplets inside yield stress materials, Phys. Rev. E **90**, 021002(R) (2014).

[33] J. B. Bostwick and P. H. Steen, Stability of constrained cylindrical interfaces and the torus lift of Plateau–Rayleigh, J. Fluid Mech. **647**, 201 (2010).

[34] H. Mehrabian and J. J. Feng, Capillary breakup of a liquid torus, J. Fluid Mech. **717**, 281 (2013).

[35] J. E. Bergen, B. C. Basso, and J. B. Bostwick, Leidenfrost drop dynamics: Exciting dormant modes, Phys. Rev. Fluids **4**, 083603 (2019).

[36] M. J. McCarthy and N. A. Molloy, Review of stability of liquid jets and the influence of nozzle design, Chem. Eng. J. **7**, 1 (1974).

[37] F. Durst, S. Ray, B. Ünsal, and O. A. Bayoumi, The development lengths of laminar pipe and channel flows, J. Fluids Eng. **127**, 1154 (2005).

[38] J. M. Bergthorson, K. Sone, T. W. Mattner, P. E. Dimotakis, D. G. Goodwin, and D. I. Meiron, Impinging laminar jets at moderate Reynolds numbers and separation distances, Phys. Rev. E **72**, 066307 (2005).

[39] C. Ellegaard, A. E. Hansen, A. Haaning, and T. Bohr, Experimental results on flow separation and transitions in the circular hydraulic jump, Phys. Scr. **1996**, 105 (1996).

[40] A. Rao and J. H. Arakeri, Wave structure in the radial film flow with a circular hydraulic jump, Exp. Fluids **31**, 542 (2001).

[41] A. R. Teymourtash and M. Mokhlesi, Experimental investigation of stationary and rotational structures in non-circular hydraulic jumps, J. Fluid Mech. **762**, 344 (2015).

[42] J. B. Bostwick and P. H. Steen, Static rivulet instabilities: Varicose and sinuous modes, J. Fluid Mech. **837**, 819 (2018).